2017•2018
Faculteit Industriële ingenieurswetenschappen
master in de industriële wetenschappen: elektronica-ICT

Masterthesis
A study ofstretchable flat spiral inductors

PROMOTOR :
Prof. dr. ir. Wim DEFERME

BEGELEIDER :
ing. Steven NAGELS

Brent Beliën

Scriptie ingediend tot het behalen van de graad van master in de industriële wetenschappen: elektronica-ICT

Gezamenlijke opleiding UHasselt en KU Leuven

2017 • 2018

Faculteit Industriële ingenieurswetenschappen

master in de industriële wetenschappen: elektronica-ICT

Masterthesis

A study ofstretchable flat spiral inductors

PROMOTOR :

Prof. dr. ir. Wim DEFERME

BEGELEIDER :

ing. Steven NAGELS

Brent Beliën

Scriptie ingediend tot het behalen van de graad van master in de industriële wetenschappen: elektronica-ICT

UHASSELT

KU LEUVEN

Preface

This thesis covers the creation and measurement of several flat spiral inductors in a stretchable substrate. It has been written as part of the industrial engineering in electronics and ICT course at the University of Hasselt in cooperation with the University of Leuven. The research and writing were conducted between January and September 2018.

The research took place in the department of functional material engineering at the institute of material research in Diepenbeek. My research was guided by my supervisors, professor Wim Deferme and Steven Nagels. There were some difficulties in this research, but I could count on their help and guidance to resolve these problems.

I would therefore like to thank my supervisors for all their help and guidance during this research. I would also like to thank the department of biomedical device engineering for letting me use their impedance analyser. I also wish to thank the departments of physics and chemistry at the University of Hasselt for letting me use their vacuum equipment. Finally, I would also like to thank Jan Boutsen for letting me use his network analyser and for giving me some more knowledge about the use of inductors in radio frequency applications. This project could never have been completed without the help of all these people.

Contents

List of Tables

List of Figures

Abstract in English

Stretchable electronics have a wide range of possible applications including soft robotics and biomedical systems. A problem with these types of devices is the power management. Contact pads on the surface of stretchable substrates can provide power but can crack and tear after a while. To solve this problem, stretchable inductors can be made which can be embedded with the circuit and provide power wirelessly. In this research, these stretchable inductors are made using laser engraving which cuts in a stretchable material known as PDMS. The design parameters of the inductor were altered to study their effects on inductance and resonance frequency. The measurements for the inductance were done with an impedance analyser and the data was analysed using the program EIS Spectrum Analyser. The resonance frequency was measured using a network analyser. From this data it is clear that the number of turns influences the inductance and resonance frequency the most. The spacing between centres of turns influences the inductance and resonance frequency to a lesser extent. The width of the conductive track of the inductor did not influence the inductance or resonance frequency at all.

Abstract in Nederlands

Rekbare elektronica heeft een breed toepassingsgebied, gaande van zachte robotica naar biomedische applicaties. Een probleem met deze apparaten is het energiebeheer. Contacten kunnen op het rekbare substraat geplaatst worden om stroom te voorzien, maar deze kunnen beschadigd worden na een tijd. Om dit probleem op te lossen kunnen er rekbare spoelen gemaakt worden die in het circuit worden verwerkt om zo draadloos stroom te kunnen voorzien. In dit onderzoek zijn er rekbare spoelen gemaakt met een lasersnijder die in een rekbaar materiaal genaamd PDMS snijdt. De ontwerpparameters van de spoelen zijn gevarieerd en het effect van deze variaties op de inductie en resonantiefrequentie van de spoel is bestudeerd. De metingen voor de inductie zijn gedaan met een impedantiemeter, deze data is dan geanalyseerd met het programma EIS Spectrum Analyser. De resonantiefrequentie is gemeten met een netwerk analyzer. Uit de data kan besloten worden dat het aantal windingen het meeste invloed heeft op de inductie en resonantiefrequentie. De afstand tussen de centers van de windingen beïnvloedt deze parameters op een mindere mate. De breedte van het geleidende pad van de spoel beïnvloedt de inductie en resonantiefrequentie helemaal niet.

Chapter 1

Introduction

In recent years the interest in stretchable, or soft, electronics has risen due to their versatility and possible applications in numerous fields. In biomedical systems, stretchable electronics can be used as part of implants in the human body, smart clothes, or even for replacing sensory organs like the eye [26, 3]. Another use of stretchable electronics lies in soft robotics, this is the use of compliant materials in robotics to operate in certain areas which would be difficult with normal robots. For example, soft robots could be used to interact with humans without harming them [31]. In this field, compliant electronics can be used to create soft sensors, soft actuators and soft power sources [21].

Currently, most conformable electronics are made with solution processing techniques such as inkjet printing [18]. With these techniques, silver particles are suspended in a solution and form a conducting path once the solvent has dried [29]. These types of stretchable electronics usually have limited stretchability and also require physical contact to charge the circuit. Conductive pads on the surface of the stretchable substrate can be used for the charging and data transfer. However, these pads can tear, crack, and can oxidise which can increase their resistance and decrease their lifespan. Another problem with the contact pads is the safety of the application, having a Galvanic isolation would decrease the risk of potential short circuits.

To solve these problems, another method for creating conformable electronics can be used. This method consists of creating microfluidic channels in a stretchable substrate, encapsulating the channels and filling them with a liquid metal. Using this method, a fully functioning and embedded electronic circuit can be created in a stretchable material. The power can be provided by inductive power transfer which also provides a Galvanic isolation. For inductive power transfer, inductors have to be used or created and embedded together with the circuit. Copper inductors are not stretchable and would be difficult to embed with the circuit. Therefore, stretchable flat spiral inductors can be made by using the microfluidic channels.

In this research several of these inductors are made using laser engraving in a stretchable material known as PDMS. The laser engraver has several properties which will be altered and their effects on the created channel's width and depth will be studied. The design parameters of the inductors will also be changed, the amount of turns, the spacing between centres of turns, and the turn width will all be altered. The effect of these parameters on the inductance and resonance frequency will be measured using an impedance analyser and a network analyser.

Chapter 2

Method

2.1 Introduction

In this chapter an in-depth analysis of the materials and methods used in this research will be given. Each section represents a step in the creation of a stretchable inductor. For each step, certain alternative materials or methods will be presented. These alternatives are used in related research, and will be compared to the ones used in this research. The theoretical basis behind some of the methods will also be explored.

2.2 Substrate materials

The first step in the creation of a stretchable inductor is getting a substrate to work with. The choice between substrates is influenced by the application for which the circuit will be used. The inductor will be used to power stretchable electronic circuits used in soft robotics or biomedical applications. Typical electronic circuits use printed circuit boards(PCB) to place and connect electrical components. These boards are rigid and sturdy which can limit their uses in applications where flexibility is required. Stretchable electronics are meant to replace these printed circuit boards because the circuits can stretch and bend, this can provide more comfort to the user of these applications.

Stretchable electronics can be made by creating stretchable structures in a metal, by creating composites, by using solution processing, or by using a liquid metal in stretchable substrates. When creating a metal into a horseshoe shaped waveform, it will let the metal stretch until the wire is straight again. There are two disadvantages with this method. One problem is that the metal has a tendency to break after a few cycles of stretching. The second problem is that the wire can only be stretched until it is straight again [20].

With composites, conductive particles are mixed with a stretchable substrate. If enough particles are inserted, they can create a conductive track trough the substrate once it has been cured [17]. A similar method for creating stretchable electronics is with solution processing. With this technique, conductive particles are mixed in with a solvent. This liquid is then used in solution processing techniques such as inkjet printing. These techniques will distribute the solvent onto the surface of a conformable material. After the solvent has dried, the silver particles will remain and will form a conducting path [18]. Both the composite technique as well as the solution processing techniques have limited stretchability. As the substrate is stretched, the distance between conductive particles will continue to increase which decreases conductivity. The particles can only be moved a certain distance from each other before all conductivity is lost.

In this research, another method for creating stretchable electronics is used. This method consists of creating microfluidic channels in a soft and stretchable substrate. These channels can then be encapsulated and filled with a liquid metal. The liquid state of the metal allows it to flow freely as the substrate is stretched. The flow of the metal will help keep a conductive track between both ends of the channel. With this technique, the conductivity will also decrease if the material is stretched because the cross-sectional area of the conductor is decreases while its length is increased. These parameters increase the resistivity R of a conductor by

$$R = \rho \cdot \frac{l}{A}, \tag{2.1}$$

where ρ is the electrical resistivity of the liquid metal, l is the length of the conductive track, and A is the cross-sectional area of the track. This relation is known as the law of Pouillet. There is also still a limit to the stretchability when using this technique, but this limit is presumably higher than the other techniques.

Materials which are currently being used as an alternative for PCBs can be classified as thin film plastics and silicone elastomers. They both have similar properties such as low cost and chemical - and temperature stability [6, 13]. However, thin film plastics are less water resistant and are also less mechanically stable because of their thinness [2]. Silicone elastomers are therefore better suited for applications involving contact with skin.

Two types of silicone elastomers are considered for this research, both are two-component polymers of a dimethylsiloxane functional group. Figure 2.1 depicts the molecular structure of this polymer which is known as polydimethylsiloxane(PDMS). The two silicones are Sylgard®184 and Shore 15, both are cured using platinum as a catalyst [23, 27]. The Shore 15 gets its name because it has a hardness of Shore A 15 and the Sylgard®184 is a brand name by Dow Corning®.

When both are mixed with their curing agent, the Sylgard®184 has a lower viscosity than the Shore 15 with a difference of 1500 mPa s^{-1} [10, 27]. Because of the lower viscosity, air pockets trapped inside the Sylgard®184 can easily escape to the surface which improves the overall quality of the cured silicone. However, the quality of the Shore 15 can be improved by putting it in a vacuum chamber to extract the air pockets. By using this technique, the Shore 15 has a quality comparable to the Sylgard®184. Because the Shore 15 is also cheaper than the Sylgard®184, the choice was made to use Shore 15 PDMS for the duration of this research.

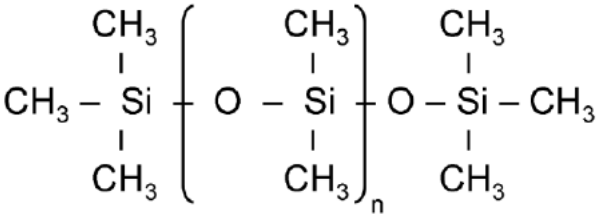

Figure 2.1: Molecular structures of PDMS [9]

In the lab, the silicone sheets are created by using blade coating to a thickness of 2 mm. First, a polymethylmethacrylate(PMMA) sheet is cleaned and sprayed with some lubricant, this is to prevent the PDMS sticking to the PMMA after it has been cured. Some silicon sealant is used to create a barrier for the PDMS, this will also give the sheet the required dimensions. Next, the PDMS is weighed and mixed with the curing agent in a 10:1 ratio. The Shore 15 has two curing agents, a fast acting agent, and a slower acting agent. The faster acting agent will give the PDMS a cure time of 15 minutes, while the slower agent will have a cure time of 6 hours. The two curing agents can be mixed to get a specific curing time [28]. Figure 2.2 depicts the curing time of the Shore 15 in relation to the ratio of fast acting agent in the total curing agent.

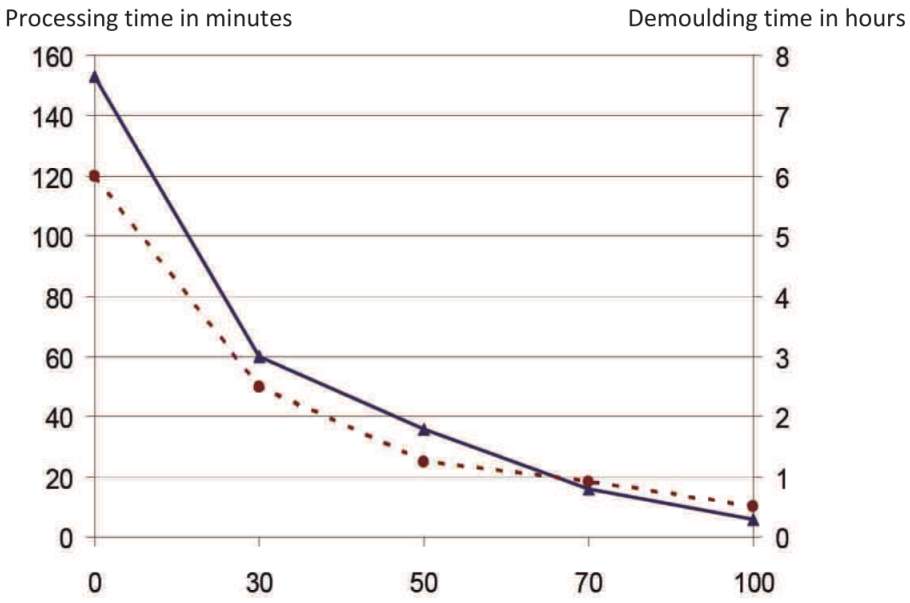

Figure 2.2: Cure time(red) and processing time(blue) in relation to ratio of fast acting agent [28]

As can be seen in figure 2.2, a mixture of 50 percent fast and 50 percent normal curing agent will result in a processing time of approximately 40 minutes. This is enough time for the blade-coating as well as the vacuum treatment. The vacuum will allow air pockets inside the PDMS to escape which will result in a better quality PDMS layer. Additionally, to further improve the quality air pockets which are still visible should be removed before curing. If too much air pockets are still present on the surface of the silicone after it has cured, then the bottom side of the sheet can be used for laser engraving.

2.3 Creating microfluidic channels

Next is the creation of the microfluidic channels in the PDMS by using laser engraving. Laser engraving was chosen because it is a cheap, fast, and easy to use method. The laser used in this research uses CO_2 as a medium for generating the laser light. CO_2 laser engraving works by electrically exciting nitrogen molecules. These excited molecules will then collide with the CO_2 molecules which in turn excites them into a metastable state. The CO_2 molecules then fall back into a stable state converting the extra energy to laser light with a wavelength of 10.6 µm [8, p. 25]. When the laser light then hits the surface of a material, its energy will get transferred to that material. If enough energy is provided, then surface material will be removed in a process which is known as laser ablation. The removal of matter from the surface is a result from photochemical or photothermal interactions. The interaction which occurs depends on the energy of the laser light and on the ablated material[8, p. 248].

The relation between the energy of a photon E and the wavelength λ of the laser light is given by

$$E = \frac{\hbar c_0}{\lambda}, \tag{2.2}$$

where $\hbar$ is Planck's constant and c_0 is the speed of light. Equation (2.2) shows that the energy of the photon increases with decreasing wavelength. If the energy of the photon exceeds the energy needed to sustain a bond between atoms, then this bond can break. These photochemical interactions typically occur in polymers and with wavelengths in the UV-spectrum. If the energy from the laser light is not enough to break the bonds, then it will be converted into heat. The heat will get absorbed by the material which increases its temperature. This local increase in temperature will cause it to melt and evaporate. Material removal using these type of interactions is known as photothermal ablation[24].

There are three types of bonds in PDMS, the silicon-oxide bond, the silicon-carbon bond, and the carbon-hydrogen bond. The average energy of these bonds are 452 kJ mol^{-1}, or 4.685 eV; 318 kJ mol^{-1}, or 3.296 eV; and 411 kJ mol^{-1}, or 4.260 eV respectively [25]. Using (2.2), the energy for a single photon of CO_2 laser light can be calculated. This energy is equal to 0.117 eV which is not enough to break any of the bonds in PDMS. Therefore, it can be concluded that PDMS structures are photothermally ablated when exposed to CO_2 laser light.

2.4 Laser properties

In the lab, the laser used to engrave the channels in the silicone is a Trotec Speedy 100R. The drivers for this machine can interpret a 2D drawing and engrave this onto the substrate. The drivers for the machine also allow the user to control certain parameters for the laser, these parameters are: laser power, laser speed, and laser pulses per inch(PPI). The laser power can be varied from 10%-100%, for this particular machine the maximum laser power is equivalent to 45 Watt [33]. Laser speed can be varied from 1%-100% of the maximum laser speed, which is 180 cm s^{-1} [33]. The last parameter is the amount of laser pulses per inch which can be varied from 500-1000, this parameter can also be exchanged for laser frequency which can be varied from 1000-60000 laser pulses per second [32].

Additionally, process parameters such as process mode and resolution can also be configured. The process mode decides how the 2D drawing is interpreted, the relief mode was chosen for this research because it varies the laser power depending on the gray-scale of the drawn object. The resolution setting determines the quality of the laser engraving, it can be varied from 125-1000 dots, or lines, per inch(DPI) [32]. A test pattern was created to examine the effects of these laser settings on channel width and depth. Figure 2.3 shows this test pattern, laser speed was kept constant at 10% of the maximum speed to reduce the amount of variables.

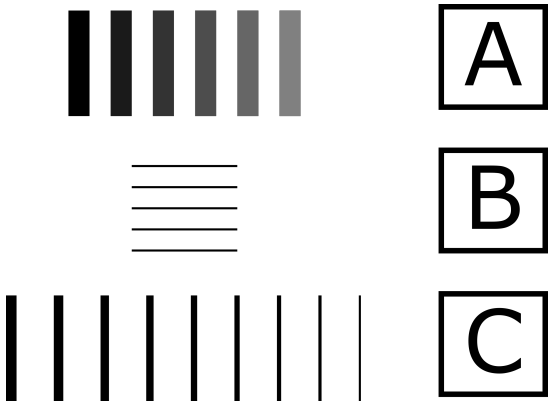

Figure 2.3: Test pattern created to test different laser settings

The first row(A) in figure 2.3 is used to test the effect of the laser power on the channel depth, the width and length are kept constant at 1 mm and 5 mm respectively. Each channel on the first row is created with a different gray-scale value, with the relief setting these channels will be engraved with a percentage of the laser power. For example, if black(0-0-0RGB) is set to be engraved with 50% of the laser power in the process parameters, then a channel created with 80% gray-scale(51-51-51RGB) is engraved with 40% of the total laser power. In the test pattern, six channels are created with gray-scale values of 100%(left) to 50%(right) in intervals of 10%.

Row B in figure 2.3 is used to test the accuracy of the laser, these channels are all created with a width of 0.1 mm which is the smallest width for the laser. Finally, the third row will test if smaller widths will result in shallower channels. The starting width is 0.5 mm and decreases with 0.05 mm for each channel until the minimum width of 0.1 mm.

2.5 Factors which influence inductance

It is important to know how the dimensions of the microfluidic channels might affect the inductance of the flat spiral inductor. For normal solenoid inductors, the number of turns, the core material, the diameter, and the spacing between turns influence the inductance the most[34, p. 314]. These parameters are also still relevant for flat spiral inductors and are incorporated in (2.3) [15]. This equation is derived from the Wheeler equation for long coils [35] but features parameters relevant for this research. Figure 2.4 shows the parameters on a cross-section of the coil.

$$L = \frac{N^2 \cdot A^2}{30A - 11D_i}, \tag{2.3}$$

$$A = \frac{D_i + N \cdot (w + s)}{2},$$

Where L = Inductance of the coil

N = Number of turns

A = Coil area

D_i = Inner diameter

w = Wire diameter

s = Spacing between turns

D_o = Outer diameter

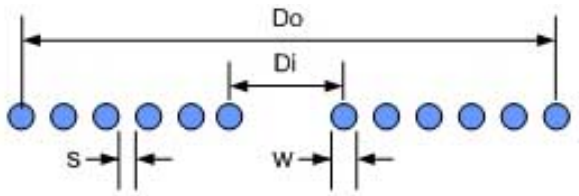

Figure 2.4: Coil parameters on a cross-section [15]

Now that all relevant parameters are known, their influence on the inductance can be found. In order to test the effect of different parameters, several inductors are created where on parameter is changed and the others are kept constant. However, there are some variables which are redefined in this research. The parameter s from figure 2.4 will be redefined to become the distance between the centres of two consecutive turns instead, defined as $t = w + s$ to avoid confusion. This avoids significant alterations to the area of the coil when testing the influence of the width on the inductance. This was done because for normal inductors, the total area also affects the inductance [34, p. 314].

The inner diameter is also different from that of figure 2.4. Because a second contact needs to be made at the center of the coil, a circular area is engraved at this location to fulfil this purpose. The distance between the edge of the circle and the next turn is defined as the inner diameter.

The last difference is the shape of the channel. For the equation the wires are assumed to be circular, but the laser engraver creates channels with a trapezoid shape. Inductors used in integrated circuits also do not have circular shaped tracks and use another modification of the Wheeler formula [22]. However, it is assumed that the thickness of the channel has no significant impact on the inductance and can therefore be neglected [22]. It is unsure if this extends to the inductors made in this research. Therefore all the inductors have been made with the same power setting to avoid altering the depth. Figure 2.5 shows an Inkscape design of the inductor with all of the parameters from (2.3) as used in this research. Table 2.1 depicts every inductor and their physical parameters which were created for this research.

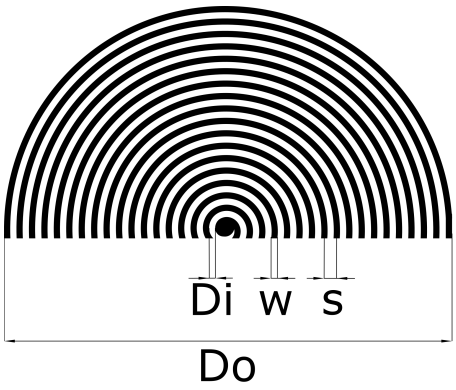

Figure 2.5: Parameters from (2.3) redefined for this research

Table 2.1: Physical parameters of all inductors

Inductor	N (turns)	w (mm)	t (mm)	D_i (mm)	D_o (mm)
1	**12**	0.7	1.4	0.7	33.3
2	**15**	0.7	1.4	0.7	42.2
3	**18**	0.7	1.4	0.7	50.5
4	**21**	0.7	1.4	0.7	58.6
5	**24**	0.7	1.4	0.7	67.5
6	18	**0.5**	1.4	0.9	50.3
7	18	**0.6**	1.4	0.8	50.3
3	18	**0.7**	1.4	0.7	50.5
8	18	**0.8**	1.4	0.6	50.5
9	18	**0.9**	1.4	0.5	50.7
3	18	0.7	**1.4**	0.7	50.5
10	18	0.7	**1.5**	0.7	54.5
11	18	0.7	**1.6**	0.7	58.3
12	18	0.7	**1.7**	0.7	61.1
13	18	0.7	**1.8**	0.7	64.8

2.6 Bonding of silicones

The laser engraving process leaves behind some residue which needs to be removed before the bonding process can begin. Removing the residue can be done by rinsing with deionised water, acetone, and isopropanol respectively and then drying with lint-free wipes. After drying, the channels can be sealed by securing a second sheet of PDMS on top of the first one. There are multiple methods which can be used to bond PDMS together, these methods can use adhesives, thermal pressure bonding, solvent bonding, ultrasonic welding, laser welding, or plasma treatments [4, 11].

Corona treatment was chosen to bond the PDMS because it is a cheap, fast, and easy to use technique which creates a decent bond. Corona treatment uses a cold air plasma at atmospheric pressure to increase the surface energy of a material. This increase in energy allows the surface to bond with other materials more easily[11]. After treatment, both sheets are laid on top of each other which creates a solid piece of PDMS with embedded microfluidic channels. The quality of the bond can be improved by working in a clean room environment which further decreases possible contamination.

2.7 Filling microfluidic channels

Filling the channels is the last step in the creation of an inductor. A liquid metal is used to fill the channels, this will allow for some stretching while still providing a conducting path. Galinstan will fulfil this purpose because it is a non-toxic metal which is liquid at room temperature. Two methods are considered for filling the channels, the first method uses a micro syringe to inject Galinstan into the channels.

First, small holes have to be drilled into the PDMS to inject the Galinstan. Injection filling requires that there are two holes one at each end of the channel, the first one is used to inject the metal and the second one is used to let the air escape. If there is no second hole, then the air cannot escape and will build up pressure which could cause the channel to burst. If the pressure applied onto the syringe is too high, then that could also cause the channel to rupture [16].

These problems can be circumvented with the second method which uses a vacuum to fill the channels. This method requires only one opening and a vacuum to fill the channels. After the hole has been drilled, Galinstan is put on top of the hole and the PDMS is put in a vacuum chamber. In the chamber, air trapped in the channels escapes trough the Galinstan. Once the vacuum is released, the pressure difference will push the metal into the channels thereby creating a filled channel [19]. A second hole is drilled at the centre of the inductor to create the second contact. The sample is put back in a vacuum chamber for a few minutes to fill the hole and provide better conductivity.

2.8 Inductor characterisation

After an inductor is filled with Galinstan, its electrical properties can be found by using an impedance measurement. The machine used for the measurement is a 4194A impedance / gain-phase analyser from Hewlett-Packard. This machine uses an I-V measurement technique to measure the impedance. An I-V measurement uses a reference resistor R_{ref} where a reference voltage V_{ref} is applied. The impedance Z can be calculated by

$$Z = \frac{V_{DUT} \cdot R_{ref}}{V_{ref}}, \tag{2.4}$$

where V_{DUT} is the voltage over the device under test(DUT)[12]. The impedance analyser is controlled using a LabVIEW program which manages the voltage, the frequency range, and saves the data in a comma separated value file. Analysis is done from 100 Hz to 40 MHz with 20 points per decade and an oscillation voltage of 0.5 V. The machine will measure the impedance and the phase of the inductor in this frequency range. To get the electrical parameters of the inductor, the measurement data will be fitted to a model of a real inductor. Figure 2.8 shows this model which is the equivalent circuit of a real inductor.

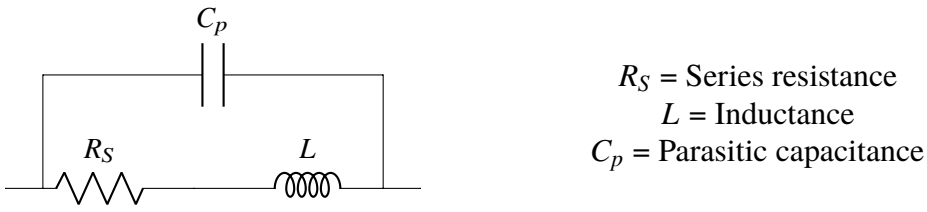

Figure 2.6: Equivalent circuit of real inductor

The model in figure 2.8 is comprised of three components, the series resistance R_S, the inductance L, and the parasitic capacitance C_p. The series resistance is at low frequencies a result of the length of the conductive path used to create the inductor, its value is determined by the conductivity of the Galinstan. At higher frequencies, losses due to skin-, proximity effects, and eddy currents contribute the most to the resistance [30]. However, at these frequencies the resistance is smaller than the inductive reactance X_L. The inductive reactance is a result of the inductor preventing the change in current when an

alternating current is applied. This property is related to the frequency of the AC signal f, and the inductance L given by 2.5.

$$X_L = 2\pi f L \tag{2.5}$$

There is also a capacitive reactance X_C which is caused by the parasitic capacitance C_p. This capacitance is the result from adding all the capacitive effects between each turns. The capacitive reactance is also related to the frequency f given by 2.6.

$$X_C = \frac{1}{2\pi f C} \tag{2.6}$$

The value of X_L is initially zero and will continue to increase with increasing frequency, while X_C is initially infinite and will continue to decrease. At a certain frequency these two values will become equal and will cancel each other out, this point is known as the resonance frequency(RF). At this point, only the resistance will contribute to the impedance. Figure 2.7 shows a typical impedance measurement of an inductor, with the impedance Z on the y-axis and the frequency f on the x-axis both in logarithmic scale.

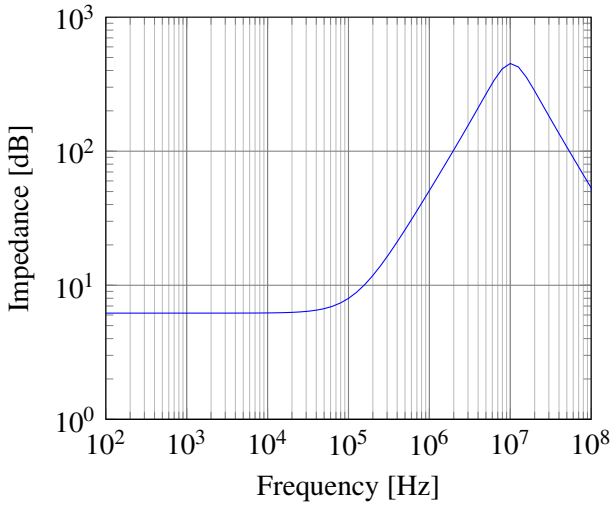

Figure 2.7: Bode plot of a real inductor

The values of L and C_p can be found by fitting this graph onto the model of a real inductor. For this research, the free to use tool EIS Analyser [5] is used for the curve fitting. Before fitting, a conversion of the data file needs to be done. The software for the impedance analyser gives the data in a comma separated value(csv) file with a header containing the details of the measurement. Two files are generated, one contains the impedance measurement and the other contains the phase measurement. The file needed for EIS analyser is a space delimited text file consisting out of three columns with the exception of the first row which has the amount of data points in the file, this can be seen in figure 2.8. After the first row, the data consists of one column with the real value of the impedance, one column with the negative imaginary value of the impedance, and one column with the frequency respectively.

n
ReZ_1 $-ImZ_1$ $Freq_1$
...
ReZ_n $-ImZ_n$ $Freq_n$

Figure 2.8: Data format for EIS analyser [5]

A MATLAB script is used to convert the csv file into a space delimited text file. The real value of the impedance is the absolute impedance multiplied with the cosine of the phase while the imaginary part is the absolute impedance multiplied with the sine of the phase. Different algorithms can be selected to try the fitting: the Nelder-Mead algorithm, Powell's algorithm, the Levenberg-Marquad algorithm,

and the Newton algorithm [5]. These curve fitting algorithms are quite complex and are beyond the scope of this project. There is also an option to give the fit an amplitude or parametric weight, but the unweighted option will be used for this research.

The impedance measurement does have some flaws, it introduces extra capacitances in the wiring and connections to the machine. These extra capacitances can result in a false reading of the resonance frequency. With the measurement parameters used in this research, the machine can only measure to a maximum frequency of 40 MHz, therefore it is possible that the resonance frequency cannot even be measured.

To solve these problems, a second measurement is done using a Hewlett Packard 8753E network analyser. The measurement works by sending a signal trough a copper inductor. This inductor is coupled with the DUT which will resist this signal and return a reflected signal. The network analyser uses the original and reflected signal to get the properties of the DUT [1]. This machine can measure up to a maximum frequency of 3 GHz and because it does not use wiring its effects on the resonance frequency are minimal. There is still the coupling capacitance between the copper inductor and the DUT, this is inevitable because a coupling is required for a measurement. By increasing the distance between the DUT and the copper inductor, the effect of the coupling capacitance can be reduced.

The resonance frequency of the inductor is also influenced by the core material. The relative permittivity of PDMS is approximately 2.7 [7, p.425] thus increasing the parasitic capacitance by a factor of 2.7 when compared to an equivalent air core inductor. The magnetic permeability of PDMS is also lower than that of air with a relative permeability of approximately 0.5 [7, p.425]. For a normal inductor, this decreased permeability would influence the inductance by

$$L_{PDMS} = \mu_{\text{PDMS}} \cdot L_{Vac}, \tag{2.7}$$

with L_{PDMS} the inductance with a PDMS core, μ_{PDMS} the permeability of PDMS, and L_{Vac} the inductance with a vacuum core which is approximately the same as an air core. These two effects combined reduce the resonance frequency of a PDMS core inductor by a factor of 0.86 when compared to an air core inductor. This relation is given by 2.8.

$$\begin{aligned} F_{Res}^{PDMS} &= \frac{1}{2\pi\sqrt{0.5 \cdot L^{Air} \cdot 2.7 \cdot C_p^{Air}}} \\ \Rightarrow F_{Res}^{PDMS} &= 0.86 \cdot F_{Res}^{Air} \end{aligned} \tag{2.8}$$

Using Galinstan instead of copper will likely not affect the inductance and therefore the resonance frequency, but will affect the resistance of the inductor. The conductivity of Galinstan is 2.30 MS m^{-1} which is 27.4 times lower than the conductivity of copper which is 63 MS m^{-1} [14].

Chapter 3

Results

3.1 Introduction

In this chapter, the results of the inductor creation and analysis will be discussed. The first section will explore the results of the test pattern. The relation between laser power and channel depth will be discussed as well as the relation between the channel width and channel depth. A second section will have the volumetric properties of the inductor, with calculations for the mass of Galinstan needed to fill each inductor. Next, the impedance analyser results will be given and the relation between the design parameters and the inductance will be discussed. The fourth section deals with the results of the network analyser results and gives the relation between the design parameters and the resonance frequency. Finally, the most prevalent failure mechanisms when creating these types of inductors will be discussed.

3.2 Test pattern results

The test pattern was used to find the influence of certain laser settings on the created channel's width and depth. The pattern was engraved a total of nine times, three times using 1000 DPI and 40% of the laser power, three times using 500 DPI and 40% of the laser power, and three times using 500 DPI and 80% of the laser power. Because the DPI determines the amount of lines engraved per inch, changing this setting will reduce the laser time on a channel which will reduce its depth. Therefore the power is increased to compensate for this decrease in depth.

The first test in the pattern consisted of varying the laser power by altering the gray-scale of the channels, this would allow the laser to engrave the channel with a percentage of power equal to that of the gray-scale percentage. This test is used to examine the effect of the laser power on the depth of the channel, but since all channels are also 1 mm wide the consistency of the width can also be examined.

The measurements for the width and depth were made using images of cross-sectional areas of the channels obtained with light microscopy. Table 3.1 shows the results for the 1000 DPI test, and table 3.2 shows the results for the 500 DPI test. Each table features the width and depth of each sample as well as their mean and standard deviation(SD for short). Figure 3.1 depicts the relation between power and depth for 1000 DPI, and figure 3.2 depicts this relation for 500 DPI.

Table 3.1: Channel depth and width in relation to the laser power with 1000 DPI

1000 DPI	Sample 1		Sample 2		Sample 3		Depth	
Laser power (%)	Depth (µm)	Width (µm)	Depth (µm)	Width (µm)	Depth (µm)	Width (µm)	Mean (µm)	SD (µm)
40	747.36	1151.97	725.58	1141.63	741.89	1145.95	738.28	11.33
36	683.79	1102.61	640.29	1156.56	640.54	1136.69	654.87	25.04
32	594.82	1098.50	538.94	1137.84	596.62	1161.52	576.79	32.79
28	500.18	1105.01	467.00	1124.14	510.93	1064.05	492.70	22.90
24	385.99	1106.20	366.82	1116.87	408.43	1094.84	387.08	20.83
20	286.81	1073.55	279.73	1125.68	307.03	1063.18	291.19	14.17

Table 3.2: Channel depth and width in relation to the laser power with 500 DPI

500 DPI	Sample 1		Sample 2		Sample 3		Depth	
Laser power (%)	Depth (µm)	Width (µm)	Depth (µm)	Width (µm)	Depth (µm)	Width (µm)	Mean (µm)	SD (µm)
80	885.55	1063.82	992.89	1169.99	894.35	1089.21	924.26	59.60
72	783.83	1193.39	894.41	1233.89	837.20	1202.17	838.48	55.30
64	741.90	1185.25	761.01	1184.39	721.14	1212.20	741.35	19.94
56	682.44	1087.98	656.28	1113.00	655.72	1165.07	664.81	15.27
48	554.33	1147.35	556.44	1169.03	512.34	1166.25	541.04	24.87
40	412.67	1128.70	424.81	1113.61	434.20	1111.17	423.89	10.79
40	409.47	1304.05	459.46	1123.01	425.68	1171.63	431.54	25.50
36	366.07	1113.87	408.11	1137.86	403.20	1176.63	392.46	22.99
32	321.00	1155.95	362.17	1158.20	336.57	1194.83	339.91	20.79
28	255.35	1103.44	305.38	1085.21	289.50	1180.61	283.41	25.56
24	204.32	1150.48	211.78	1122.91	209.37	1130.62	208.49	3.81
20	139.51	1111.48	147.00	1068.94	130.19	1072.16	138.90	8.42

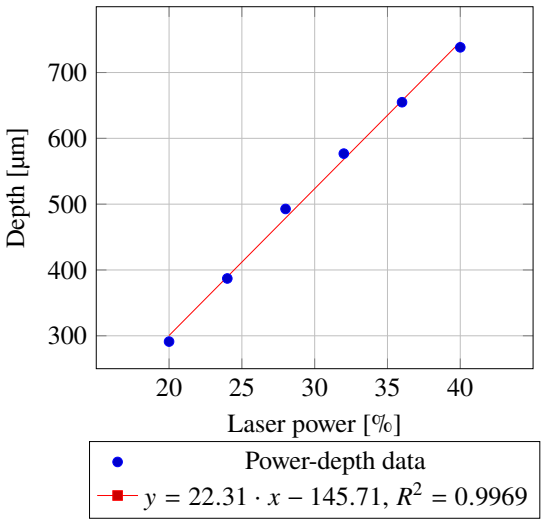

Figure 3.1: Depth of a channel in function of the percentage of laser power for 1000DPI

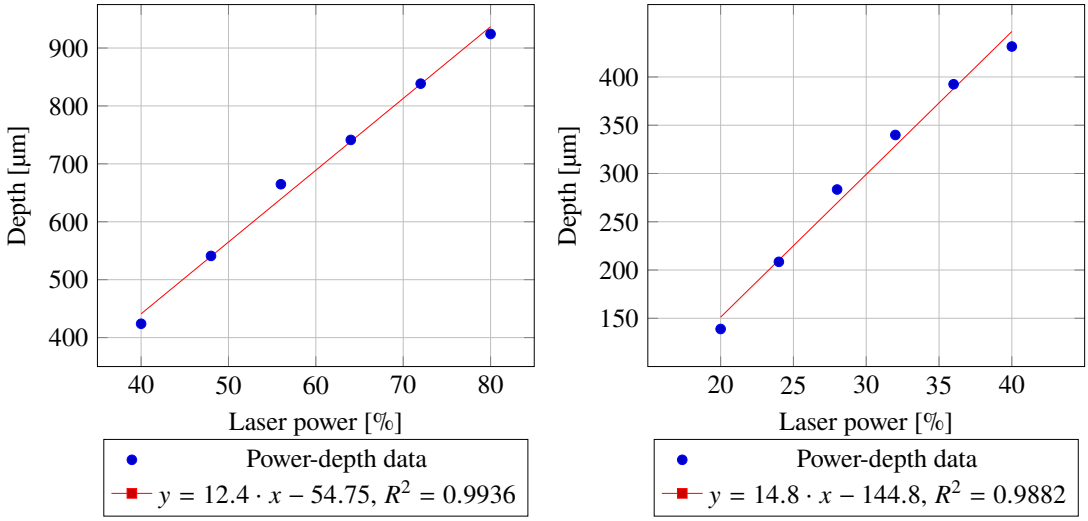

Figure 3.2: Depth of a channel in function of the percentage of laser power for 500 DPI

In figures 3.1 and 3.2, linear trend lines have been added to determine the linearity of the power-depth relation. The coefficient of determination(R^2) is in all three instances practically one, which implies that the power and depth are indeed linearly related. Another conclusion is the reduction in depth when the resolution is changed. The channels engraved at 500 DPI are 60% as deep as those engraved at 1000 DPI when both are using 40% of the total laser power. Doubling the power to 80% on 500 DPI therefore does not result in the same depth as the ones with 1000 DPI and 40% power. To get approximately the same depth, a power setting of 65%-70% should be used.

Tables 3.1, and 3.2 include the width of each channel, from which the consistency and error for the laser can be extracted. The average width is 1117.04 ± 30.73 µm for channels engraved with 1000 DPI, this is an 11.70% error compared to the 1 mm design. The channels engraved with 500 DPI and 40% power have an average width of 1142.32 ± 54.59 µm equal to an error of 14.23%, and the channels with 80% power have an average width of 1152.03 ± 47.74 µm with an error of 15.20%. From this data it can be concluded that the actual engraved width has a relatively small error compared to what is drawn. This error also has a small increase when the DPI is lowered, and the deviation is also a bit higher than that of the 1000 DPI channels. For the remaining experiments and for the inductors, the resolution has been set at 1000 DPI and the laser power at 40%. These settings were chosen because they had the most consistent results.

The next test that was included in the test pattern also tested the consistency of the laser engraver. However, this test has the channels designed to be 0.1mm which is the smallest width the laser can engrave. Table 3.3 depicts the width and depth measurements of five channels from two samples.

Table 3.3: Consistency of the laser for 0.1mm channels on 1000 DPI with 40% power

1000 DPI	Sample 1			Sample2		
Design width (µm)	Width (µm)	Error (%)	Depth (µm)	Width (µm)	Error (%)	Depth (µm)
100	279.99	179.99	543.79	318.94	218.94	521.76
100	290.85	190.85	561.23	302.73	202.73	564.888
100	276.15	176.15	541.6	300.08	200.08	539.8
100	280.12	180.12	596.17	310.84	210.84	524.15
100	289.34	189.34	560.25	336.66	236.66	541.51

Averaging out the values from table 3.3 results in a width of 298.57 ± 19.35 µm and a depth of 549.51 ± 21.94 µm. The error on the width is 198.57%, which is greater than the approximate 10% of the 1 mm channels. Besides this error, the width appears to be consistent with a 6.48% deviation from the average. It should also be mentioned that the average depth for a 100 µm channel is lower than that of a 1 mm channel while both are engraved with the same power setting. This would imply that there is a relation between the width and the depth of a channel, this relation is tested in the final experiment of the test pattern. Table 3.4 contains the results from this test, and figure 3.3 shows these results graphically.

Table 3.4: Channel width and depth relation on 1000 DPI with 40% power

1000 DPI	Sample 1			Sample 2			Depth		Width	
Design width (µm)	Depth (µm)	Width (µm)	Error (%)	Depth (µm)	Width (µm)	Error (%)	Mean (µm)	SD (µm)	Mean (µm)	SD (µm)
100	518.26	216.64	116.64	561.05	212.44	112.44	539.66	30.26	214.54	2.97
150	683.28	343.92	129.28	719.22	324.73	116.49	701.25	25.41	334.33	13.57
200	738.83	350.55	75.28	762.31	338.62	69.31	750.57	16.60	344.59	8.44
250	803.32	497.49	99.00	816.54	442.30	76.92	809.93	9.35	469.90	39.03
300	796.68	499.75	66.58	881.21	493.72	64.57	838.95	59.77	496.74	4.26
350	800.97	511.91	46.26	874.56	518.92	48.26	837.77	52.04	515.42	4.96
400	792.56	609.20	52.30	866.32	520.27	30.07	829.44	52.16	564.74	62.88
450	796.02	594.23	32.05	763.83	589.49	31.00	779.93	22.76	591.86	3.35
500	773.47	724.43	44.89	813.96	622.17	24.43	793.72	28.63	673.30	72.31

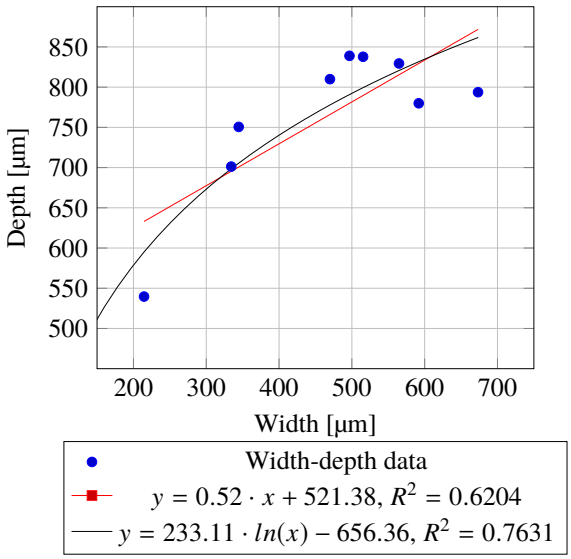

Figure 3.3: Depth of a channel in function of the width of the channel with 1000DPI and 40% power

In figure 3.3 a linear and logarithmic trend line are added to examine the relation between the width and depth of a channel. The coefficient of determination is higher for the logarithmic trend line than the one for the linear trend line. This indicates that the relation between width and depth is more logarithmic. This claim is supported by the depth data in table 3.1, where a channel with the same power setting and a width of 1145.95 µm is 738.28 µm deep. Therefore, it can be assumed that the width only influences the depth when the engraved width is lower than 500 µm. In table 3.4 it can also be seen that the error to the design is larger below this threshold. Figure 3.4 depicts the cross-sectional areas of these channels, with the most narrow channel on the left and the widest on the right. Note that the shape of the channel transitions from triangular to trapezoid when the width increases which could explain the increased error. Figure 3.5 is a cross-section of a defective inductor which is shaped as a trapezoid with bases $B1$ and $B2$, and a height of H.

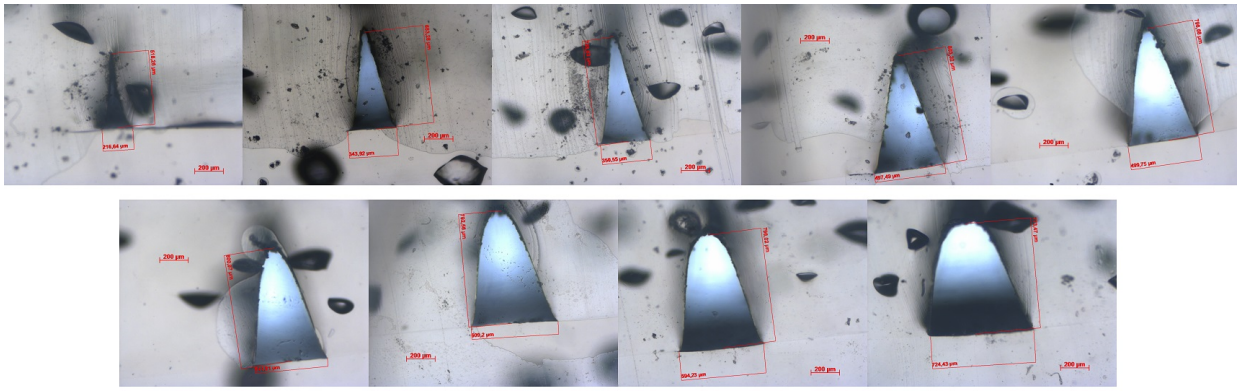

Figure 3.4: Cross-section of channels for the width-depth relation

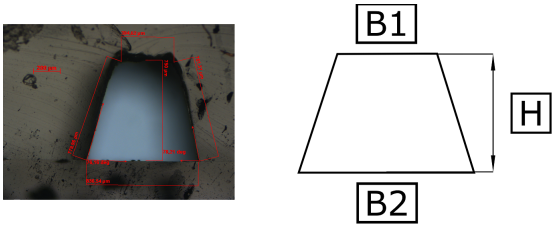

Figure 3.5: Cross-section of defective inductor channel

3.3 Characterisation results

3.3.1 Volumetric calculations

For filling the inductors, it is helpful to get an estimation on the amount of Galinstan needed to fill them. For calculating this volume, a couple of assumptions have to be made. First, the cross-sectional area of the inductor is assumed to be trapezoid like in figure 3.5. The length of the top part of the trapezoid(B1) is approximately half that of the bottom part(B2), but is assumed half for the calculations. The cross-sectional area A_c of a trapezoid can be found by

$$A_c = \frac{B1 \cdot B2}{2} \cdot H \qquad [\text{mm}^2], \tag{3.1}$$

where $B1$ is the top base of the trapezoid which is half that of the bottom base $B2$, and H is the distance between both bases. This distance is the depth with which the channel is engraved and is assumed to be 738.28 µm. The bottom base is the width of the channel and is assumed to be equal to the design width.

Next, an approximation of the length l of a coil can be made by

$$l = \frac{\frac{D_o^2}{4} \cdot \pi}{t} \qquad [\text{mm}], \tag{3.2}$$

where D_o is the outer diameter of the inductor, and t is the distance between the centres of two consecutive turns. Finally, the volume V of the air inside the inductor can be calculated by multiplying A_c with l. Multiplying this result with the density of Galinstan, which is 6.44 g cm^{-3} [14], will give the mass of the Galinstan inside the inductor once it is filled. Table 3.5 depicts the results of these calculations for all the inductors.

Table 3.5: Volumetric properties of all inductors

Inductor	N (turns)	w (mm)	t (mm)	D_i (mm)	D_o (mm)	l (mm)	A_c (mm^2)	V (cm^3)	m (g)
1	**12**	0.7	1.4	0.7	33.3	622.09	0.0904	0.0562	0.3622
2	**15**	0.7	1.4	0.7	42.2	999.05	0.0904	0.0903	0.5816
3	**18**	0.7	1.4	0.7	50.5	1430.69	0.0904	0.1293	0.8329
4	**21**	0.7	1.4	0.7	58.6	1926.45	0.0904	0.1742	1.1215
5	**24**	0.7	1.4	0.7	67.5	2556.05	0.0904	0.2311	1.4881
6	18	**0.5**	1.4	0.9	50.3	1419.38	0.0461	0.0654	0.4214
7	18	**0.6**	1.4	0.8	50.3	1419.38	0.0664	0.0942	0.6069
3	18	**0.7**	1.4	0.7	50.5	1430.69	0.0904	0.1293	0.8329
8	18	**0.8**	1.4	0.6	50.5	1430.69	0.1181	0.1690	1.0881
9	18	**0.9**	1.4	0.5	50.7	1442.04	0.1495	0.2156	1.3884
3	18	0.7	**1.4**	0.7	50.5	1430.69	0.0904	0.1293	0.8329
10	18	0.7	**1.5**	0.7	54.5	1555.22	0.0904	0.1406	0.9054
11	18	0.7	**1.6**	0.7	58.3	1668.43	0.0904	0.1508	0.9713
12	18	0.7	**1.7**	0.7	61.1	1724.74	0.0904	0.1559	1.0041
13	18	0.7	**1.8**	0.7	64.8	1832.18	0.0904	0.1656	1.0667

3.3.2 Impedance analyser results

The impedance was measured using a 4194A impedance/gain-phase analyser from Hewlett-Packard, the machine can measure impedance up to 40 MHz. The connectors and cables that are used in this measurement have capacitances which obscures the real resonance frequency. However, for some inductors it was apparent that the resonance peak could not be measured due to the limited range of the machine. Therefore, a capacitance of 33 nF was added in parallel to the inductor which decreased the resonance frequency to a point where it was measurable. Table 3.6 shows the results of these measurements.

Table 3.6: Impedance analyser results

Inductor	N (turns)	w (mm)	t (mm)	D_i (mm)	D_o (mm)	F_{res}^{imp} (MHz)	L_{calc} (µH)	R_s^K (Ω)
1	**12**	0.7	1.4	0.7	33.3	0.4833	3.2859	0.84
2	**15**	0.7	1.4	0.7	42.2	0.3830	5.2303	4.33
3	**18**	0.7	1.4	0.7	50.5	0.3411	6.5988	1.81
4	**21**	0.7	1.4	0.7	58.6	0.3411	6.5988	3.00
5	**24**	0.7	1.4	0.7	67.5	0.2407	13.252	3.60
6	18	**0.5**	1.4	0.9	50.3	0.3411	6.5988	3.30
7	18	**0.6**	1.4	0.8	50.3	0.3411	6.5988	2.41
3	18	**0.7**	1.4	0.7	50.5	0.3411	6.5988	1.81
8	18	**0.8**	1.4	0.6	50.5	0.3411	6.5988	1.36
9	18	**0.9**	1.4	0.5	50.7	0.3831	5.3203	1.29
3	18	0.7	**1.4**	0.7	50.5	0.3411	6.5988	1.81
10	18	0.7	**1.5**	0.7	54.5	0.3411	6.5988	1.98
11	18	0.7	**1.6**	0.7	58.3	0.3411	6.5988	2.52
12	18	0.7	**1.7**	0.7	61.1	0.3036	8.3254	8.51
13	18	0.7	**1.8**	0.7	64.8	0.3411	6.5988	2.08

In table 3.6 F_{res}^{imp} denotes the resonance frequency with the 33 nF capacitance. L_{calc} is the inductance calculated by

$$L_{calc} = \frac{1}{(2 * \pi * F_{res}^{imp})^2 \cdot C_{add}}, \tag{3.3}$$

where C_{add} is the 33 nF capacitance. This calculation gives an estimation on the real value of the inductance, it is not exact as the capacitance is not exactly 33 nF. R_s^K is the series resistance, measured with a 4 point resistance measurement and a Keithley 2000 multimeter. The data files from the impedance measurement are converted and used in the EIS analyser, the equivalent circuit of an inductor is used for fitting. The Newton algorithm with the unweighted function is used to fit the data to the model. Table 3.7 depicts the result of the fitting.

For the values of the inductance L^{EIS}, parasitic capacitance C_p^{EIS}, and the series resistance R_s^{EIS} there is a percentage error given by EIS analyser. This error is the difference between the calculated values and the data from the measurement [5], and is converted to a deviation. Now, the relation between the parameters and the inductance can be found. First is the relation between the amount of turns N and the inductance L^{EIS}, this relation is illustrated in figure 3.6(A).

Theoretical values for the inductance are also included in table 3.7, these are calculated by using equation 2.3 and the parameters from table 2.1. These values do not differ much from the EIS obtained inductance which disproves the assumption that the inductance of PDMS cores is only half that of air cores. It is likely that the PDMS covering the channels is not thick enough to cause a large deviation in inductance when compared to normal air core inductors.

Table 3.7: EIS analyser results

Inductor	L^{EIS} (µH)	C_p^{EIS} (nF)	R_s^{EIS} (Ω)	L_{theory} (µH)
1	3.652 ± 0.055	30.893 ± 0.044	2.452 ± 0.142	1.703
2	4.119 ± 0.400	30.426 ± 0.176	10.541± 0.394	3.281
3	7.002 ± 0.067	30.590 ± 0.028	3.164 ± 0.132	5.617
4	5.588 ± 0.230	30.594 ± 0.135	4.151 ± 0.340	8.861
5	10.000 ± 0.076	30.871 ± 0.057	3.359 ± 0.215	13.16
6	6.944 ± 0.090	30.630 ± 0.037	3.833 ± 0.1677	5.692
7	6.765 ± 0.117	31.253 ± 0.051	3.701 ± 0.220	5.655
3	7.002 ± 0.067	30.590 ± 0.028	3.164 ± 0.132	5.617
8	6.721 ± 0.076	30.971 ± 0.034	2.774 ± 0.155	5.580
9	6.682 ± 0.026	30.121 ± 0.205	2.746 ± 0.067	5.542
3	7.002 ± 0.067	30.590 ± 0.028	3.164 ± 0.132	5.617
10	6.949 ± 0.101	31.120 ± 0.043	3.365 ± 0.195	6.000
11	7.201 ± 0.124	31.151 ± 0.051	3.848 ± 0.227	6.382
12	7.732 ± 0.300	30.031 ± 0.090	9.334 ± 0.346	6.765
13	7.740 ± 0.102	30.930 ± 0.039	3.334 ± 0.186	7.147

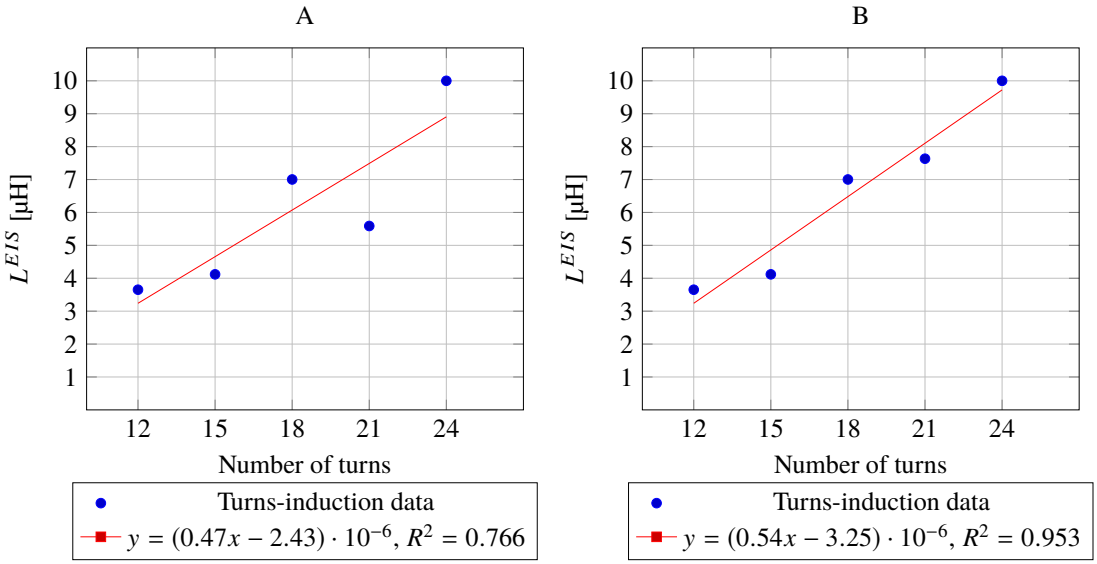

Figure 3.6: Induction in function of the amount of turns (A), and modified version (B)

From figure 3.6(A) it is clear that that inductor 4, which is the inductor with 21 turns, does not fit the linear trend from the other data points. Figure 3.7(A), shows the fit for this inductor in EIS analyser. Note that the calculated impedance spectrum has a deviation from the data. This deviation can be reduced by adding a resistor R_p parallel to the inductor [1], the new calculated spectrum is depicted in

figure 3.7(B). It is apparent that this fit is better than the previous one, the parameter values have also changed: $L^{EIS} = 7.633 \pm 0.360\mu H$, $C_p^{EIS} = 26.86 \pm 0.117nF$, $R_s^{EIS} = 2.869 \pm 0.482\Omega$, and $R_p^{EIS} = 50.315 \pm 7.969\Omega$.

Figure 3.6(B) shows the induction in function of the number of turns with the modification of inductor 4. The coefficient of determination is now closer to one, this suggests that the inductance and the number of turns are linearly related. Only inductor 4 required this particular model, all other inductors used the default model of a real inductor.

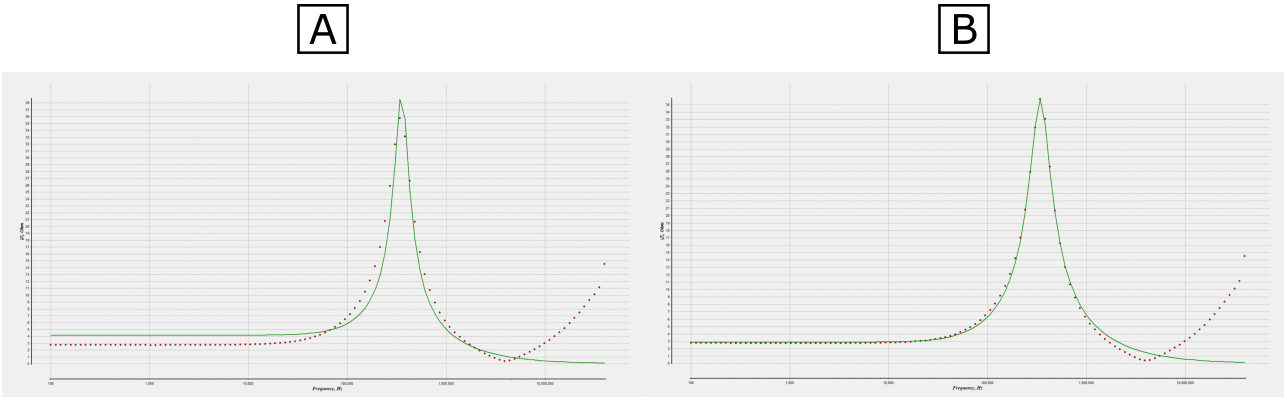

Figure 3.7: Inductor 4 comparison of different fitting models

The second relation which was studied, was the relation of the width w and the induction L^{EIS} which is illustrated in 3.8(A). Finally, the relation betweeen the turn spacing t and the inductance L^{EIS} is shown in figure 3.8(B).

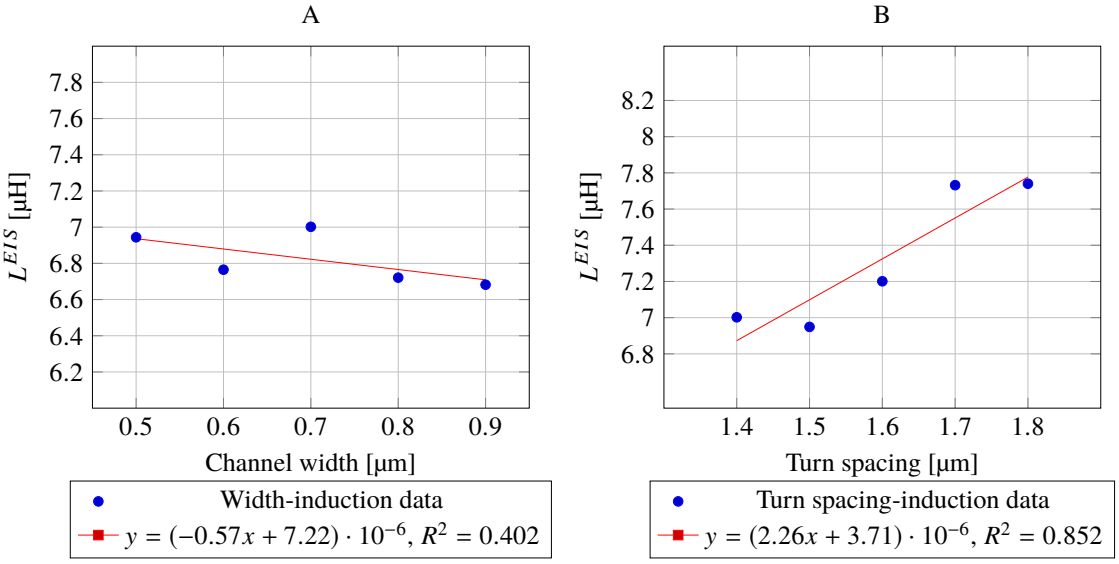

Figure 3.8: Induction in function of the width of the channel (A), and in function of spacing between turns (B)

From figure 3.8(A) it can be seen that R^2 is relatively low which indicates that there is no linear relation between the width and the induction. Averaging out the values for the inductance when the width is varied gives an inductance of 6.823 ± 0.142 µH. The low deviation suggest that the inductance remains nearly constant as the width is varied which further suggest that they are not related. This result is to be expected with the definition of the turn spacing $t = w + s$. Using this definition in the equation for the

inductance of flat spiral inductors results in

$$L = \frac{N^2 \cdot A^2}{30A - 11D_i},$$
$$A = \frac{D_i + N \cdot (t)}{2},$$

where L is now independent of the width. However, it was unsure whether this equation holds true for inductors made with laser engraving and filled with Galinstan. The inner diameter D_i does still change as it is the same as s. It is likely that the influence of this parameter on the inductance is small enough where it gets cancelled out by imprecisions of the measurement and the EIS analyser.

The turn spacing does have an influence on the inductance as can be seen in figure 3.8(B). The relation was tested with a linear, logarithmic, and exponential trend which have an coefficient of determination of 0.852, 0.840, and 0.853 respectively but a linear trend was chosen because it is the most probable.

3.3.3 Vector network analyser results

For accurately measuring the resonance frequency of the inductor, a Hewlett Packard 8753E network analyser is used. A copper inductor is used to couple with the DUT, and is placed 0.5 cm under the DUT to minimize the coupling capacitance. The resonance frequency of the DUT is measured in 5 different position, the top side F_{res}^{t}, the left side F_{res}^{l}, the bottom side F_{res}^{b}, the right side F_{res}^{r} and the centre F_{res}^{c}. The resonance frequency has a slight deviation in these different positions and by averaging them to F_{res}^{avg}, a better result can be obtained. Table 3.8 shows the results of these measurements. Figure 3.9(A) depicts the relation between the amount of turns and F_{res}^{avg}, figure 3.10(A) illustrates the relation between the width of a channel and F_{res}^{avg}, and figure 3.10 (B) shows the relation between the turn spacing and F_{res}^{avg}.

Table 3.8: Vector network analyser results

Inductor	F_{res}^{t} (MHz)	F_{res}^{l} (MHz)	F_{res}^{b} (MHz)	F_{res}^{r} (MHz)	F_{res}^{c} (MHz)	F_{res}^{avg} (MHz)
1	125.915	125.975	124.77	123.74	126.055	125.291 ± 1.015
2	104.660	104.505	103.955	103.365	104.306	104.158 ± 0.516
3	56.175	56.855	56.853	56.820	56.610	56.663 ± 0.291
4	157.719	160.680	161.513	159.151	156.969	159.206 ± 1.918
5	32.828	32.708	32.786	32.011	32.453	32.557 ± 0.338
6	59.928	59.894	59.894	59.572	59.938	59.845 ± 0.154
7	58.014	57.972	57.828	57.420	58.016	57.850 ± 0.252
3	56.175	56.855	56.853	56.820	56.610	56.663 ± 0.291
8	56.983	56.99	56.860	56.985	56.995	56.963 ± 0.058
9	60.280	60.193	60.098	60.143	60.190	60.181 ± 0.068
3	56.175	56.855	56.853	56.820	56.610	56.663 ± 0.291
10	54.230	54.227	54.281	54.179	54.293	54.242 ± 0.046
11	51.221	51.263	51.212	51.239	51.206	51.228 ± 0.023
12	48.698	48.644	48.467	48.686	48.623	48.624 ± 0.093
13	47.201	47.162	47.024	47.093	47.177	47.131 ± 0.072

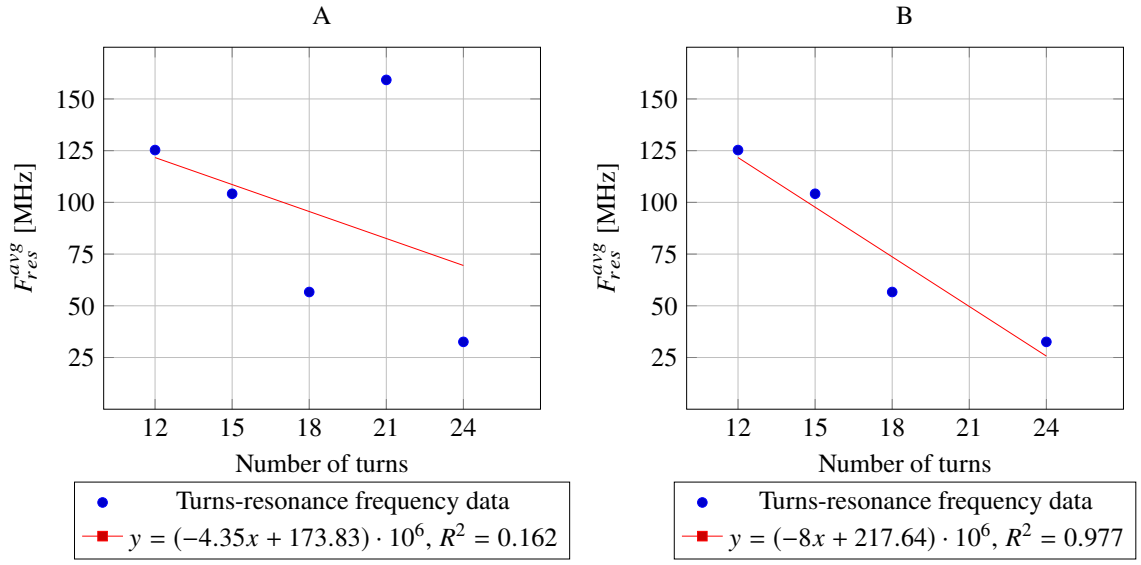

Figure 3.9: Resonance frequency in function of the number of turns (A), with inductor 4 omitted (B)

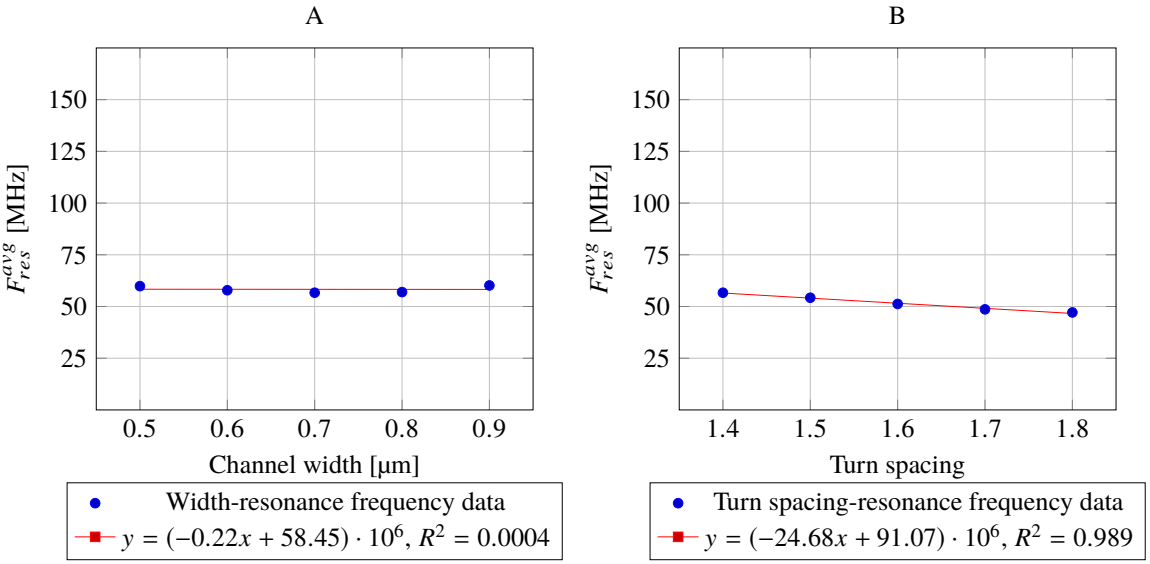

Figure 3.10: Resonance frequency in function of the channel width (A), and in function of turn spacing (B)

Similar to the impedance analyser results, inductor 4 does not follow the trend of the other four inductors. Omitting this inductor from the results yields a better coefficient of determination that is approximately one which can be seen in figure 3.9(B). The relation between the number of turns and the resonance frequency can therefore be assumed to be linear.

Another similarity with the impedance results is the relation between the width of a channel and the resonance frequency which is to say that there is no relation. The resonance frequency remains constant at a 58.3 ± 1.63MHz and the coefficient of determination is also essentially zero which further confirms that there is no relation between width and inductance or resonance frequency. Finally, the relation between the turn spacing and the resonance frequency is linear which corresponds with the results from the impedance analyser.

3.3.4 Summary of results

All the results are summarized in table 3.9 where L^{EIS} is the induction calculated from the EIS analysis, F_{res}^{avg} is the average resonance frequency of the inductor, C_{calc} is the parasitic capacitance calculated using

$$C_{calc} = \frac{1}{(2 * \pi * F_{res}^{avg})^2 \cdot L^{EIS}}, \tag{3.4}$$

and R_s^K is the DC resistance of the inductor. The deviations of L^{EIS} and F_{res}^{avg} can be found in table 3.7 and 3.8 respectively.

Table 3.9: Summary of the inductors and their electrical properties

Inductor	N (turns)	w (mm)	t (mm)	F_{res}^{avg} (MHz)	L^{EIS} (µH)	C_{calc} (pF)	R_s^K (Ω)
1	**12**	0.7	1.4	125.291	3.652	0.442	0.84
2	**15**	0.7	1.4	104.158	4.119	0.567	4.33
3	**18**	0.7	1.4	56.663	7.002	1.127	1.81
4	**21**	0.7	1.4	159.206	5.588	0.179	3.00
5	**24**	0.7	1.4	32.557	10.000	2.39	3.60
6	18	**0.5**	1.4	59.845	6.944	1.019	3.30
7	18	**0.6**	1.4	57.85	6.765	1.119	2.41
3	18	**0.7**	1.4	56.663	7.002	1.127	1.81
8	18	**0.8**	1.4	56.963	6.721	1.162	1.36
9	18	**0.9**	1.4	60.181	6.682	1.047	1.29
3	18	0.7	**1.4**	56.663	7.002	1.127	1.81
10	18	0.7	**1.5**	54.242	6.949	1.239	1.98
11	18	0.7	**1.6**	51.228	7.201	1.34	2.52
12	18	0.7	**1.7**	48.624	7.732	1.386	8.51
13	18	0.7	**1.8**	47.131	7.740	1.473	2.08

With this data, it is possible to construct an inductor with a desired inductance or resonance frequency and approximate the amount of turns and turn spacing it needs. For example, an inductor with an induction of 6 µH is needed. Using inductor 3 as a base line, its induction is calculated to be 6.47 µH when using the equation for the trend line from figure 3.6(B). From this equation it is also known that adding or subtracting a turn from the design changes the inductance with 0.54 µH. The influence of the turn spacing is less with a 0.226 µH change in induction when altering the spacing with 0.1 mm.

There are multiple options to get the desired result, the first one is a reduction of one turn which results in an induction of 5.93 µH. The second option is to reduce the amount of turns by two, and increase the turn spacing with 0.3 mm resulting in an induction of 6.068 µH. The final option is to decrease the turn spacing by 0.2 mm which has an inductance of 6.018 µH.

It is also possible to calculate the resonance frequency and the parasitic capacitance using these custom parameters. The resonance frequency changes with 8 MHz for each change in the number of turns, and with 2.468 MHz for each change of 0.1 mm to the turn spacing. The base line resonance frequency of inductor 3 is calculated to be 73.64 MHz with a capacitance of 0.722 pF. The resonance frequency becomes 65.64 MHz for the first solution, 65.044 MHz for the second solution, and 68.704 MHz for the final solution. The capacitances for these solutions are 0.991 pF, 0.987 pF, and 0.892 pF respectively.

3.4 Failure mechanisms

During this research, the inductors were made by using several techniques together, this can cause some problems and lead to damaged, or incomplete inductors. An example of such an error is during the first step of inductor creation, the silicon blade-coating. The silicon sheets that were made in this research were all intended to be 2 mm thick, a thick layer of silicon makes it easier to handle and improves the sturdiness of the inductor. However, it is possible that the sheet is thinner than 2 mm due to a wrong setting of the blade coater or by not pouring enough silicone. From table 3.1 can be seen that a channel engraved with 40% laser power has a depth of 738.28 ± 11.33 µm. A large deviation could therefore cause the laser to burn trough the silicone sheet and destroy the inductor.

The depth of the channel and thickness of the silicone are also another problem when using the inductor in stretchable applications. Preferably, the total thickness of the finished inductor should be 2 mm or less to keep sufficient stretchability. This limits the thickness of each sheet to 1 mm which makes a reduction of laser power essential. A laser power of 28% or less is recommended when using this thickness because it engraves at a depth of approximately 500 µm. This also reduces the amount of particles in the channel which makes it easier to clean and also decreases the chance of particles interfering with the bonding or filling.

Another benefit of reducing the laser power is the decrease in air volume. This decreases the time the inductor needs to stay in a vacuum and decreases the amount of Galinstan needed to fill the inductor. However, decreasing the thickness of the sheets may make it more difficult to operate with. A solution to this could be to first pour a thick silicon sheet and pour a thin layer on top of it. When the inductor needs to be used in an application, the two layers can be separated and only the thin layer is used.

A second example of a potential failure is during corona bonding. It is possible that during the bonding process, air pockets can get caught between the two sheets. It is important to remove these air pockets as they can cause the sheets to delaminate and can cause Galinstan overflowing during filling. The overflowing occurs when the inductor is put in a vacuum for filling, after releasing the vacuum it is possible that because of delamination the Galinstan will flow over the channel and into the next as seen in figure 3.11(A).

Other errors can also occur in the filling process, one such an error is the incomplete filling of a channel. Figure 3.11(B) shows an example of this error, it can occur when the vacuum is released too soon and not enough air has escaped. Another error is that not enough Galinstan is pushed into the channel which causes an air gap with Galinstan on both sides like in figure 3.11(C). This occurs when the pressure is restored and not enough Galinstan remains on the hole to fill the entire inductor. The last error occurs after the second hole has been made, the inductor is put in a vacuum again to get lower resistance. It is possible that certain channels will overflow if the inductor is put in a vacuum for too long.

When altering the parameters to influence the inductance, there are some limits to what is realistically possible to create. In this research inductors have been made with less than 1.4 mm turn spacing, this yielded fragile inductors which could easily tear. This could possibly be resolved by decreasing laser power, but decreasing t too much could also increase the chance of Galinstan overflowing. Conversely, increasing t too much may make it impractical to implement into certain applications as increasing t also increases the total area. This is also true for increasing the number of turns, these two also have another side effect which is the increased Galinstan required to fill the channels. Increasing the size of the inductor also increases the time needed to engrave them. Because the width does not seem to influence the inductance, having a small width therefore reduces the amount of Galinstan needed to fill the channel. It is not recommended to reduce the width below 0.5 mm as this could alter the shape and depth of the channels.

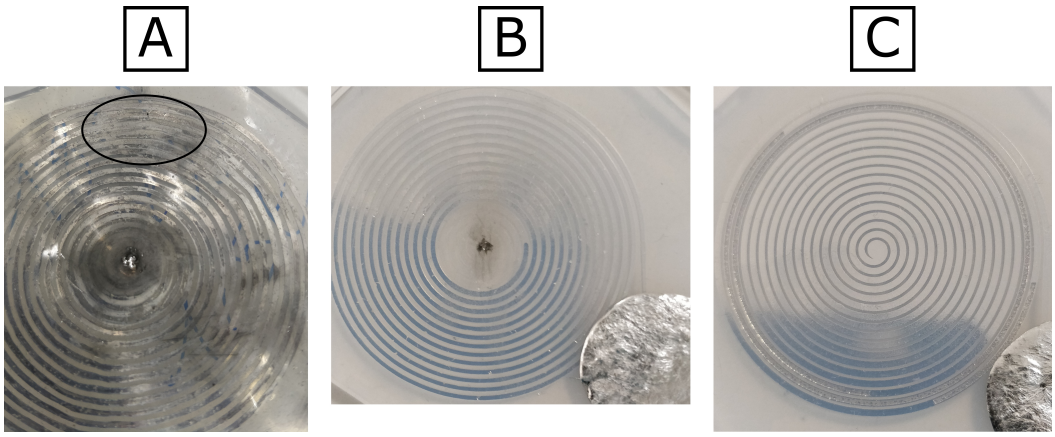

Figure 3.11: Common errors during filling, Galinstan leak (A), incomplete filling (B), air pockets in channel (C)

Chapter 4

Conclusion

In this research, several stretchable flat spiral inductors have been made and characterised. The inductors were created for use in stretchable electronic applications, they could be used for powering the circuit and even for data transfer. To make the inductors stretchable, a material known as Shore 15 Polydimethylsiloxane was used. The silicone was mixed with a curing agent in a 10:1 ratio and blade-coated to a thickness of 2 mm. After curing, a laser engraver was used to photothermally ablate the inductor in this layer of silicone. A second layer of silicone was then used to seal the inductor after it was cleaned from the laser residue. To finish the inductor, all the air in the channels was extracted in a vacuum chamber and was refilled with a liquid metal known as Galinstan. Using an impedance analyser and a network analyser, the inductance and the resonance frequency of the inductor were measured.

Before creating the inductors, the effect of different laser setting on the channel dimensions was examined. A first experiment tested the increase of laser power and its effect on the depth of the channel. Several samples engraved with a resolution of 1000 DPI, 500 DPI, and 500 DPI using double power were created for this experiment. It was concluded that with a 1000 DPI resolution, each percentage increase in laser power engraved the channel 22.31 µm deeper while only 12.4-14.8 µm with a 500 DPI resolution. Additionally, it was found that using 500 DPI resulted in channels which were 60% less deep than once with 1000 DPI. A resolution of 1000 DPI, and a laser power of 40% were used for creating the inductors and the additional tests.

The second test was used to examine the accuracy of the laser when engraving its theoretical limit of 0.1 mm wide channels. The results of the test showed that there was an 198.57% error with the 0.1 mm design which was a large increase compared to the 10% error when engraving 1 mm wide channels. Finally, it was also tested if the width of a channel would influence its depth. The results showed that this relation was logarithmic in nature, and that after a width of 0.5mm the depth would not be influenced anymore.

Several parameters of the inductor design were altered to study their effects on the inductance and resonance frequency. The altered parameters consisted of the number of turns N, the width of the channel w, and the spacing between the centres of two consecutive turns t. One parameter is altered at a time while the others remain constant. The amount of turns are changed from 12 to 24 in steps of 3 turns while t and w remained 1.4 mm and 0.7 mm respectively. From the measurements it was concluded that adding one turn increases the inductance with 0.54 µH and decreases the resonance frequency with 8 MHz. There was an exception to this trend, the inductor with 21 windings had a lower inductance and higher resonance frequency than was expected. It is possible that there was an error in the creation of this inductor, or that these specific parameters cause this deviation. Nevertheless, more research could be done to find the true cause of this anomaly.

The turn spacing was altered from 1.4 to 1.8 mm in steps of 0.1 mm while N remained constant at 18 turns, and w was 0.7 mm. A 0.1 mm change in the turn spacing resulted in a change of 0.226 µH in inductance and a 2.468 MHz change in resonance frequency. The width was altered from 0.5 to 0.9 mm in steps of 0.1 mm, and had a constant 18 turns and 1.4 mm turn spacing. Changes in the width did not affect the inductance or resonance frequency at all, both remaining constant at with a 6.823 ± 0.142 µH inductance and a 58.3 ± 1.63 MHz resonance frequency.

Looking at the equation for the inductance of flat spiral inductors

$$L = \frac{N^2 \cdot A^2}{30A - 11D_i},$$
$$A = \frac{D_i + N \cdot (t)}{2},$$
$$t = w + s,$$

it is clear that there are similarities with the data from this research. First, the amount of turns has the most influence on the inductance and the turn spacing has a smaller influence. With the definition of t the width does not have an influence at all because the spacing between turns s is altered in an equal but opposite manner to keep t constant. This is also consistent with the data from this research. The inner diameter D_i is equal to s and also changes when w is changed. If the effects of w and s are assumed to cancel each other, then the effect of D_i is also negligible because the inductance and resonance frequency are not affected. However, it is possible that the measuring equipment is not sensitive enough to measure the influence of this parameter. Additional research can be done to find the effect of D_i, s, and w on the inductance and the resonance frequency.

Using the equation, the inductance for normal air core flat spiral inductors with the same parameters can be calculated. The results of these calculations show that the inductance is not greatly affected by the use of PDMS and Galinstan. PDMS does have a relative magnetic permeability which is half that of air which would decrease the inductance by half when uses as a core. However, it is likely that the layer of PDMS is thin enough which limits its affect on the inductance. PDMS also has a relative permittivity which is 2.7 times that of air which would increase the capacitive effects with the same factor. Additional research could be done to find out if PDMS does influence the capacitance this much, and to find out its actual influence on the inductance.

The inductors created in this research are not ideal for use in stretchable electronics, they have a thickness of around 4 mm which limits their stretchability. Additionally, their thickness could also be problematic when embedding them with a stretchable electronic circuit. Reducing the thickness of the silicone also requires a reduction in laser power to compensate. This has some additional benefits such as reduced vacuum time and reduced Galinstan volume. However, the influence of the depth on the inductance is unknown and could cause irregularities.

Besides the thickness, the size of the inductors should also be taken into consideration when using them in stretchable applications. The total area of the inductor is influenced by the amount of turns and the turn spacing. Reducing these parameters results in a smaller area but also decreases the inductance and increases the resonance frequency. Conversely, increasing the parameters increases the inductance and decreases the resonance frequency but may make it more impractical to implement these applications.

Bibliography

[1] Agilent. “Agilent Impedance Measurement Handbook A guide to measurement technology and techniques”. In: *Measurement* (2009), p. 140. ISSN: 5950-3000.

[2] All Flex Inc. *polyimide vs silicone for flexible heaters*. URL: https://www.allflexinc.com/blog/polyimide-vs-silicone-for-flexible-heaters/.

[3] F. Axisa et al. “Biomedical stretchable sytems using mid based stretchable electronics technology”. In: *Annual International Conference of the IEEE Engineering in Medicine and Biology - Proceedings* (2007), pp. 5687–5690. ISSN: 05891019. DOI: 10.1109/IEMBS.2007.4353637.

[4] Holger Becker and Claudia Gärtner. “Polymer microfabrication technologies for microfluidic systems”. In: *Analytical and Bioanalytical Chemistry* 390.1 (2008), pp. 89–111. ISSN: 16182642. DOI: 10.1007/s00216-007-1692-2.

[5] Alexander S. Bondarenko and Genady A. Ragoisha. *EIS Spectrum Analyser*. 2005. URL: http://www.abc.chemistry.bsu.by/vi/analyser/.

[6] O J Cain. “Plastic substrates for thin film electronic devices”. In: *Thin Solid Films* 2.5 (1968), pp. 479–486. ISSN: 0040-6090. DOI: https://doi.org/10.1016/0040-6090(68)90061-8.

[7] Polymer Class. “Polymer Data”. In: *October* (1999), p. 1264. ISSN: 0002-7863. DOI: 10.1021/ja907879q. URL: http://www.lavoisier.fr/livre/notice.asp?id=OR6WARASROROWA.

[8] Narendra B. Dahotre and Sandip P. Harimkar. *Laser fabrication and manufacturing of materials*. 2008, pp. 3–31. ISBN: 9780387723433.

[9] V Danilov et al. “Plasma treatment of polydimethylsiloxane thin films studied by infrared reflection absorption spectroscopy”. In: 1.July 2009 (2009), pp. 2–5.

[10] Dow Corning. “Product Information: Dow Corning 184 Silicone Elastomer”. In: (2010), pp. 1–3.

[11] D. P. Dowling and C. P. Stallard. “Achieving enhanced material finishing using cold plasma treatments”. In: *Transactions of the IMF* 93.3 (2015), pp. 119–125. ISSN: 0020-2967. DOI: 10.1179/0020296715Z.000000000240. URL: http://www.tandfonline.com/doi/full/10.1179/0020296715Z.000000000240.

[12] V Dumbrava and L Svilainis. “Uncertainty analysis of I-V impedance measurement technique”. In: ().

[13] Stockwell elastomerics. “Silicone Sponge and Silicone Rubber Gaskets, Seals, Cushions, and Materials Why Use Silicone Rubber? Material Properties of Silicone Rubber Long Term Compression Set Resistance”. In: (). URL: https://www.stockwell.com/data-sheets/silicone-materials-guide.pdf.

[14] Geratherm Medical AG. “Safety Data Sheet acc , to Guideline 93 / 112 / EC”. In: (2004), pp. 2004–2007.

[15] Tesla institute. *Flat spiral coil inductor calculator*. URL: http://www.tesla-institute.com/!app/sim/fscic.php.

[16] Sang Woo Jin et al. “Stretchable Loudspeaker using Liquid Metal Microchannel”. In: *Scientific Reports* 5 (2015), pp. 1–13. ISSN: 20452322. DOI: 10.1038/srep11695. URL: http://dx.doi.org/10.1038/srep11695.

[17] Alexandre Larmagnac et al. “Stretchable electronics based on Ag-PDMS composites”. In: *Scientific Reports* 4.1 (2015), p. 7254. ISSN: 2045-2322. DOI: 10.1038/srep07254. URL: http://www.nature.com/articles/srep07254.

[18] Toni Liimatta et al. “Inkjet printing in manufacturing of stretchable interconnects”. In: *Proceedings - Electronic Components and Technology Conference* (2014), pp. 151–156. ISSN: 05695503. DOI: 10.1109/ECTC.2014.6897281.

[19] Yiliang Lin et al. “Vacuum filling of complex microchannels with liquid metal”. In: *Lab Chip* 17 (2017), pp. 3043–3050. ISSN: 1473-0197. DOI: 10.1039/C7LC00426E. URL: http://xlink.rsc.org/?DOI=C7LC00426E.

[20] Thomas Loher et al. “Stretchable electronic systems for wearable and textile applications”. In: *IEEE 9th VLSI Packaging Workshop in Japan, VPWJ 2008* (2008), pp. 9–12. DOI: 10.1109/VPWJ.2008.4762190.

[21] Nanshu Lu and Dae-Hyeong Kim. “Flexible and Stretchable Electronics Paving the Way for Soft Robotics”. In: *Soft Robotics* 1.1 (2014), pp. 53–62. ISSN: 2169-5172. DOI: 10.1089/soro.2013.0005. URL: http://online.liebertpub.com/doi/abs/10.1089/soro.2013.0005.

[22] Sunderarajan S Mohan et al. “Simple Accurate Expressions for Planar Spiral Inductances”. In: 34.10 (1999), pp. 1419–1424.

[23] Denisse Ortiz-Acosta. “Sylgard® Cure Inhibition Characterization”. In: (2012). DOI: 10.2172/1053123. URL: http://www.osti.gov/servlets/purl/1053123/.

[24] Mohammadreza Riahi. “CO2 Laser and Micro-Fluidics”. In: *Intechopen* (2009), p. 308.

[25] CD Schaeffer and CA Strausser. “Data for General, Organic, and Physical Chemistry”. In: *Franklin & Marshall . . .* (1989). URL: http://w1.vscht.cz/ktk/www%7B%5C_%7D324/lab/texty/ana/data.pdf.

[26] Paul J Shaw et al. “Materials and Mechanics for Stretchable Electronics”. In: 287.5459 (2017), pp. 1834–1837.

[27] Silicones and more. “Product Information Silicones”. In: (). URL: https://www.siliconesandmore.com/en/silicones-addition-transparent-15-normal.html.

[28] Silicones and more. *Silicone addition transperent 15(1.1 kg)*. URL: https://www.siliconesandmore.com/en/silicones-addition-transparent-15-normal.html?id=60394415%7B%5C&%7Dquantity=1%7B%5C&%7Dcustom%7B%5C%%7D255B2427536%7B%5C%%7D255D=.

[29] Jari Suikkola et al. “Screen-Printing Fabrication and Characterization of Stretchable Electronics”. In: *Scientific Reports* 6.1 (2016), p. 25784. ISSN: 2045-2322. DOI: 10.1038/srep25784. URL: http://www.nature.com/articles/srep25784.

[30] Niranjan A. Talwalkar, C. Patrick Yue, and S. Simon Wong. “Analysis and synthesis of on-chip spiral inductors”. In: *IEEE Transactions on Electron Devices* 52.2 (2005), pp. 176–182. ISSN: 00189383. DOI: 10.1109/TED.2004.842535.

[31] Deepak Trivedi et al. “Soft robotics: Biological inspiration, state of the art, and future research”. In: *Applied Bionics and Biomechanics* 5.3 (2008), pp. 99–117. ISSN: 17542103. DOI: 10.1080/11762320802557865.

[32] Trotec Produktions- und Vertriebs GmbH. “Operation manual”. In: (2009), pp. 1–31.

[33] Trotec Produktions- und Vertriebs GmbH. “TECHNICAL SPECIFICATION 8010 Speedy 100 R”. In: 43.0 ().

[34] Neville Van Valkenburgh Nooger. *Basic electricity : complete course*. English. Rev. ed. Index. Rochelle Park, N.J. : Heyden Book Company, 1980.

[35] Harold A. Wheeler. “Simple inductance formulas for radio coils”. In: *Proceedings of the Institute of Radio Engineers* 16.10 (1928), pp. 1398–1400. ISSN: 07315996. DOI: 10.1109/JRPROC.1928.221309.

Auteursrechtelijke overeenkomst

Ik/wij verlenen het wereldwijde auteursrecht voor de ingediende eindverhandeling:
A study of stretchable flat spiral inductors

Richting: **master in de industriële wetenschappen: elektronica-ICT**
Jaar: **2018**

in alle mogelijke mediaformaten, - bestaande en in de toekomst te ontwikkelen - , aan de Universiteit Hasselt.

Niet tegenstaand deze toekenning van het auteursrecht aan de Universiteit Hasselt behoud ik als auteur het recht om de eindverhandeling, - in zijn geheel of gedeeltelijk -, vrij te reproduceren, (her)publiceren of distribueren zonder de toelating te moeten verkrijgen van de Universiteit Hasselt.

Ik bevestig dat de eindverhandeling mijn origineel werk is, en dat ik het recht heb om de rechten te verlenen die in deze overeenkomst worden beschreven. Ik verklaar tevens dat de eindverhandeling, naar mijn weten, het auteursrecht van anderen niet overtreedt.

Ik verklaar tevens dat ik voor het materiaal in de eindverhandeling dat beschermd wordt door het auteursrecht, de nodige toelatingen heb verkregen zodat ik deze ook aan de Universiteit Hasselt kan overdragen en dat dit duidelijk in de tekst en inhoud van de eindverhandeling werd genotificeerd.

Universiteit Hasselt zal mij als auteur(s) van de eindverhandeling identificeren en zal geen wijzigingen aanbrengen aan de eindverhandeling, uitgezonderd deze toegelaten door deze overeenkomst.

Voor akkoord,

Beliën, Brent

Datum: **22/08/2018**